Journal of Sound and Vibration 382 (2016) 274–290

Contents lists available at ScienceDirect

Journal of Sound and Vibration

journal homepage: www.elsevier.com/locate/jsvi

A dynamic model of a cantilever beam with a closed, embedded horizontal crack including local flexibilities at crack tips

J. Liu [a,b,c,*], W.D. Zhu [c,**], P.G. Charalambides [c], Y.M. Shao [a], Y.F. Xu [c], X.M. Fang [c]

[a] State Key Laboratory of Mechanical Transmission, Chongqing University, Chongqing 400030, PR China
[b] College of Mechanical Engineering, Chongqing University, Chongqing 400030, PR China
[c] Department of Mechanical Engineering, University of Maryland Baltimore County, Baltimore, MD 21250, USA

ARTICLE INFO

Article history:
Received 22 December 2014
Received in revised form
16 April 2016
Accepted 29 April 2016
Handling Editor: I. Trendafilova
Available online 6 July 2016

Keywords:
Vibration
Cracked cantilever beam
Fully embedded horizontal crack
Closed crack
J-integral
Three-segment beam model

ABSTRACT

As one of major failure modes of mechanical structures subjected to periodic loads, embedded cracks due to fatigue can cause catastrophic failure of machineries. Understanding the dynamic characteristics of a structure with an embedded crack is helpful for early crack detection and diagnosis. In this work, a new three-segment beam model with local flexibilities at crack tips is developed to investigate the vibration of a cantilever beam with a closed, fully embedded horizontal crack, which is assumed to be not located at its clamped or free end or distributed near its top or bottom side. The three-segment beam model is assumed to be a linear elastic system, and it does not account for the nonlinear crack closure effect; the top and bottom segments always stay in contact at their interface during the beam vibration. It can model the effects of local deformations in the vicinity of the crack tips, which cannot be captured by previous methods in the literature. The middle segment of the beam containing the crack is modeled by a mechanically consistent, reduced bending moment. Each beam segment is assumed to be an Euler–Bernoulli beam, and the compliances at the crack tips are analytically determined using a *J*-integral approach and verified using commercial finite element software. Using compatibility conditions at the crack tips and the transfer matrix method, the nature frequencies and mode shapes of the cracked cantilever beam are obtained. The three-segment beam model is used to investigate the effects of local flexibilities at crack tips on the first three natural frequencies and mode shapes of the cracked cantilever beam. A stationary wavelet transform (SWT) method is used to process the mode shapes of the cracked cantilever beam; jumps in single-level SWT decomposition detail coefficients can be used to identify the length and location of an embedded horizontal crack.

1. Introduction

Embedded cracks are one of major failure modes of mechanical structures subjected to periodic loads. The dynamic characteristics and the safety of machineries are greatly affected by cracks due to fatigue. To prevent catastrophic failure of

** Corresponding author. Tel.: +1 410 455 3394.
* Corresponding author at: State Key Laboratory of Mechanical Transmission, Chongqing University, Chongqing 400030, PR China. Tel.: +86 23 65112520.
E-mail addresses: jliu@cqu.edu.cn (J. Liu), wzhu@umbc.edu (W.D. Zhu).

http://dx.doi.org/10.1016/j.jsv.2016.04.036
0022-460X/

machineries, mechanical structure monitoring for early crack detection and diagnosis is an important task for industrial maintenance.

When a crack occurs in a structure, its static and dynamic characteristics such as the stiffness, natural frequencies, mode shapes, damping, and vibration amplitudes will be changed [1,2]. An investigation of changes in the static and dynamic characteristics makes it possible to detect a crack in a structure [1–4]. While mode shapes and damping are more sensitive to the existence of a crack in a structure than natural frequencies in practice, magnitudes of changes in the natural frequencies are also functions of the severity and location of the cack in the structure [2,5–10]. Many research works determine damage severity of beam structures using analytical, numerical, and experimental methods. For an open crack, damage detection depends on changes in the static and dynamic characteristics. For a breathing crack, it depends on nonlinear dynamic characteristics, such as periodical structural stiffness variation, modulation frequencies, and higher harmonics, which was discussed in Ref. [11].

As one of accurate and comprehensive methods, a modeling and simulation method can predict the dynamic characteristics of a cracked structure and provide some guidance to early detection of crack failure. Many previous works focused on an edge crack [9,12–24] and multiple edge cracks [3,10,25–30] in cantilever or simply supported beams. Some researchers have studied delaminations in beam structures [16,31–46]. While some studies [33,34,41,43,46] are focused on detection of delamination in a laminated material, some [4,16,31,32,35–38,40,42,44,45] are focused on modeling delaminations in beam structures based on analytical methods, the finite element (FE) method, and experimental methods. The compatibility conditions at the junctions are formulated as changes in the axial forces and bending moments there [16,31,32,35–37,39,40,42,44], which cannot describe local flexibilities at crack tips due to the presence of a crack. Wang and Qiao [38] used a shear compliance coefficient at a crack tip to describe the crack tip deformation for a simply-supported end-notched beam specimen. Qiao and Chen [45] used the model in Ref. [38] to study deformations at delamination tips in a clamped and a simply supported bi-layer composite beam with an interface delamination. Cantilever beam structures with embedded cracks have not been discussed in the literature.

In this work, a new three-segment beam model with local flexibilities at crack tips is developed to investigate the vibration of a cantilever beam with a closed, fully embedded horizontal crack, which is assumed to be not located near its clamped or free end or distributed near its top or bottom side. For the closed, fully embedded horizontal crack, the top and bottom segments always stay in contact at their interface and have the same transverse displacements; they can slide over each other in the axial direction except at their ends. Such a crack can occur in a layered structure prone to delamination. While the beam is assumed to be homogeneous here, the methodology developed in this work can be extended to laminates with homogeneous layers, whose material properties are not functions of spatial variables. Hence, the three-segment beam model is assumed to be a linear elastic system and does not account for the nonlinear crack closure effect. The proposed model can describe the effects of local deformations in the vicinity of the crack tips, which cannot be captured by previous analytical methods in the literature. The middle segment of the beam containing the crack has a mechanically consistent, reduced bending moment. This work builds on parallel studies in Ref. [47] where the macro-mechanics of a cantilever beam with an embedded horizontal crack under a static load is addressed. Each beam segment is assumed to be an Euler–Bernoulli beam in this work, which implies that it is slender. However, the methodology developed here can be extended to the case where each beam segment is modeled as a Timoshenko beam. Compliances at the crack tips are analytically determined using a *J*-integral approach [48]. The *J*-integral approach may not be used to analyze a breathing, embedded crack with opening and closing states, or a crack located near the clamped or free end of the beam, or distributed near its top or bottom side. Using compatibility conditions at the crack tips and the transfer matrix method [18,27,49], the natural frequencies and mode shapes of the cracked cantilever beam are obtained. Since the FE method has been widely used in deformation and vibration studies of beams with cracks [1,22,42,50–56], the *J*-integral and stress state results from the analytical method are verified using commercial FE software [57]. A more detailed comparison of the *J*-integral results using the analytical and FE methods is presented in Ref. [47].

The new three-segment beam model is used to investigate the effects of local flexibilities at crack tips on the first three natural frequencies and mode shapes of the cracked cantilever beam. The results show that the model put forward here is an improvement over the related one, where crack-induced rotational flexibilities of cross-sections of the beam at the crack tips are not considered. As will be demonstrated later in this study, inclusion of local flexibilities at the crack tips can model

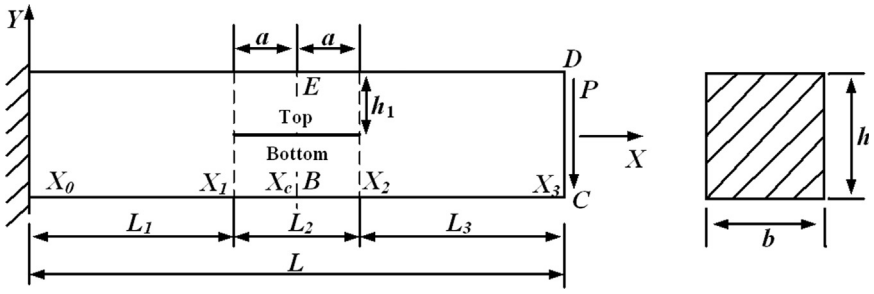

Fig. 1. Schematic of a cantilever beam with a closed, fully embedded horizontal crack.

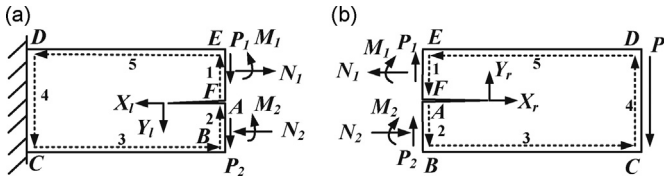

Fig. 2. Two parts of the cracked beam and paths used in determining the *J*-integrals along the contours of the (a) left (FEDCBA) and (b) right (ABCDEF) parts of the beam.

kinks in mode shapes there. A stationary wavelet transform (SWT) method [58,59] is used to process mode shapes of the cracked cantilever beam; it is shown that jumps in single-level SWT decomposition detail coefficients can be used to identify the location and size of an embedded horizontal crack. This study is a first step towards modeling and detecting a slant crack in a beam structure.

2. Crack-induced local flexibilities at crack tips

A uniform Euler–Bernoulli cantilever beam of length L, height h, and width b with a closed, fully embedded horizontal crack is shown in Fig. 1, where P is an applied force, X_0 and X_3 are the fixed and free ends of the beam, respectively, and X_1 and X_2 represent the end points of the crack relative to the global X–Y coordinates. The crack length is L_2 and the crack depth from the top surface of the beam is h_1 with $0<h_1<h$. It is assumed that the center of the crack is located at X_c with $L_2/2<X_c<L-L_2/2$. The beam is divided into three segments of lengths L_1, L_2, and L_3, which are separated by the end points of the crack.

The equivalent crack-induced rotational flexibilities of cross-sections of the beam at the two crack tips are analytically determined here using a *J*-integral approach. The beam is divided into two parts at the center of the crack, as shown in Fig. 2, where P_1 and P_2 are the shear forces on the edges EF and AB, respectively, M_1 and M_2 are the bending moments at EF and AB, respectively, and N_1 and N_2 are the axial forces acting at the centroids of the top and bottom cross-sections of the beam at the center of the crack, respectively. The *J*-integrals along the contours of the left (FEDCBA) and right (ABCDEF) parts of the beam are determined in what follows. The local coordinates for the left and right parts of the beam are shown in Fig. 2.

According to Rice's method [48], a *J*-integral is given by

$$J=\int_{\Gamma}\left(W\,\mathrm{d}Y-T_i\frac{\partial u_i}{\partial x}\mathrm{d}s\right) \tag{1}$$

where the Einstein summation convention is used; W is the strain energy density; Γ is a curve surrounding a crack tip; $T_i=\sigma_{ij}n_j$ are components of the traction vector, in which σ_{ij}, with $i,j=1,2$ for a planar problem, are stress components, and n_j are components of the outward normal along Γ; u_i are components of the displacement vector; $\mathrm{d}Y$ is a length element along the Y_r or Y_l axis in the local coordinates, as shown in Fig. 2; and $\mathrm{d}s$ is an arc length element along Γ. For the right part of the beam in Fig. 2(b), the *J*-integral along the contour ABCDEF is the sum of line integrals along segments AB, BC, CD, DE, and EF of the contour:

$$J^r=J^r_{AB}+J^r_{BC}+J^r_{CD}+J^r_{DE}+J^r_{EF} \tag{2}$$

where the superscript r denotes the right part. For segments BC and DE, $\mathrm{d}Y=0$ and $T_i=0$; hence

$$J^r_{BC}=0,\quad J^r_{DE}=0 \tag{3}$$

For segment AB, one has

$$J^r_{AB}=\int_{AB}\left(W^r_{AB}\,\mathrm{d}Y-T_i\frac{\partial u_i}{\partial x}\mathrm{d}s\right)=\int_{AB}\left(-W^r_{AB}\,\mathrm{d}s-\left(T_1\frac{\partial u^r_1}{\partial X}+T_2\frac{\partial u^r_2}{\partial X}\right)\mathrm{d}s\right) \tag{4}$$

where

$$W^r_{AB}=\frac{1}{2}\sigma^r_{xx2}\varepsilon^r_{xx2}+\frac{1}{2}\tau^r_{xy2}\gamma^r_{xy2} \tag{5}$$

in which σ^r_{xx2} and τ^r_{xy2} are the normal and shear stresses on segment AB, respectively, ε^r_{xx2} and γ^r_{xy2} are the normal and shear strains of segment AB, respectively, and the subscript 2 denotes the stress and strain components associated with segment AB. They are given by

$$\begin{aligned}\sigma^r_{xx2}&=\frac{N_2}{A_b}-\frac{M_2}{I_b}Y,\quad \epsilon^r_{xx2}=\frac{\partial u^r_1}{\partial X}=\frac{N_2}{EA_b}-\frac{M_2}{EI_b}Y\\ \tau^r_{xy2}&=\frac{P_2S(Y)}{I_bt_1},\quad \gamma^r_{xy2}=\frac{\tau^r_{xy2}}{G}=\frac{\partial u^r_1}{\partial Y}+\frac{\partial u^r_2}{\partial X}=\frac{P_2S(Y)}{GI_bt_1}\end{aligned} \tag{6}$$

where E and G are the elastic and shear moduli of the beam, respectively, A_b is the cross-sectional area of the bottom segment of X_1X_2, I_b is the cross-sectional area moment of inertia of the bottom segment of X_1X_2 about its centroidal axis, X

and Y are the displacements in the X and Y directions, respectively, $S(Y)=\int Y\mathrm{d}A$, in which $\mathrm{d}A$ is an element area, and u_1^r and u_2^r are the deflections of the bottom segment of X_1X_2 in the X and Y directions, respectively. The relationship between the deflections in the X and Y directions is [60]

$$u_1^r = u_1^{0r} - \frac{\partial u_2^{0r}}{\partial X} Y \tag{7}$$

where the superscript 0 denotes deflections along the centroidal axis of the bottom segment of X_1X_2. Differentiating Eq. (7) with respect to Y yields

$$\frac{\partial u_1^r}{\partial Y} = -\frac{\partial^2 u_2^{0r}}{\partial X \partial Y} Y - \frac{\partial u_2^{0r}}{\partial X} = -\frac{\partial u_2^{0r}}{\partial X} = -\frac{\partial u_2^r}{\partial X} \tag{8}$$

where $\frac{\partial^2 u_2^{0r}}{\partial X \partial Y} = 0$ since the slope of the deflection along the centroidal axis of the bottom segment of X_1X_2 does not depend on Y. As discussed in Ref. [47], for the cracked cantilever beam, the deflection angle of the cross-section AB can be assumed to be the sum of the deflection angle of the cross-section at X_1 relative to that at X_0 and the deflection angle of the cross-section at X_c relative to that at X_1:

$$\frac{\partial u_2^r}{\partial X} = -\frac{PL_1^2}{2EI} - \frac{P(L-L_1)L_1}{EI} - \frac{P_2 a^2}{2EI_b} + \frac{M_2 a}{EI_b} \tag{9}$$

where $a=0.5L_2$ (Fig. 1). Then

$$\gamma_{xy2}^r = \frac{\partial u_2^r}{\partial X} = -\frac{PL_1^2}{2EI} - \frac{P(L-L_1)L_1}{EI} - \frac{P_2 a^2}{2EI_b} + \frac{M_2 a}{EI_b} \tag{10}$$

The traction vector components for segment AB are given by

$$T_1 = \sigma_{11} n_1 + \sigma_{12} n_2 = -\sigma_{11}, \quad T_2 = \sigma_{21} n_1 + \sigma_{22} n_2 = -\sigma_{21} \tag{11}$$

Use of Eqs. (5)-(10) in Eq. (4) yields

$$\begin{aligned} J_{AB}^r &= \int_{BA} \frac{1}{2} \sigma_{xx2}^r \epsilon_{xx2}^r \mathrm{d}Y + \int_{BA} \tau_{xy2} \frac{\partial u_2^r}{\partial X} \mathrm{d}Y \\ &= \frac{N_2^2}{2EA_b} + \frac{M_2^2}{2EI_b} + \frac{PP_2L_1^2}{2EI} + \frac{PP_2(L-L_1)L_1}{EI} + \frac{P_2^2 a^2}{2EI_b} + \frac{P_2 M_2 a}{EI_b} \end{aligned} \tag{12}$$

Similarly, the line integral along segment EF is

$$J_{EF}^r = \frac{N_1^2}{2EA_t} + \frac{M_1^2}{2EI_t} + \frac{PP_1L_1^2}{2EI} + \frac{PP_1(L-L_1)L_1}{EI} + \frac{P_1^2 a^2}{2EI_t} + \frac{P_1 M_1 a}{EI_t} \tag{13}$$

where A_t is the cross-section area of the top segment of X_1X_2, and I_t is the cross-sectional area moment of inertia of the top segment of X_1X_2 about its centroidal axis. For segment CD

$$J_{CD}^r = \int_{CD} W_{CD}^r \mathrm{d}Y - T_i \frac{\partial u_i}{\partial X} \mathrm{d}s = \int_{CD} \left(W_{CD}^r - \left(T_1 \frac{\partial u_1^r}{\partial X} + T_2 \frac{\partial u_2^r}{\partial X} \right) \right) \mathrm{d}s \tag{14}$$

where

$$W_{CD}^r = \frac{1}{2} \sigma_{xx4}^r \varepsilon_{xx4}^r + \frac{1}{2} \left(\tau_{xy4}^r \varepsilon_{xy4}^r + \tau_{yx4}^r \varepsilon_{yx4}^r \right) = \frac{1}{2} \sigma_{xx4}^r \varepsilon_{xx4}^r + \frac{1}{2} \tau_{xy4}^r \gamma_{xy4}^r \tag{15}$$

in which the subscript 4 denotes the stress and strain components associated with segment CD. The normal stress, normal strain, shear stress, and shear strain for segment CD are given by

$$\begin{aligned} \sigma_{xx4}^r(y) = 0, \quad \varepsilon_{xx4}^r(y) = \frac{\sigma_{xx4}^r}{E} = \frac{\partial u_1^r}{\partial X} = 0 \\ \tau_{xy4}^r = \frac{PS(Y)}{It_1}, \quad \gamma_{xy4}^r = \frac{\tau_{xy4}^r}{G} = \frac{\partial u_1^r}{\partial Y} + \frac{\partial u_2^r}{\partial X} = \frac{PS(Y)}{GIt_1} \end{aligned} \tag{16}$$

The rotational angle of the cross-section CD is assumed to be the sum of the rotational angle of the cross-section at X_1 relative to that at X_0, the rotational angle of the cross-section at X_2 relative to that at X_1 for either the top or bottom segment of X_1X_2 since the top and bottom segments have the same rotational angles at X_1 and X_2, and the rotational angle of the cross-section at X_3 relative to that at X_2:

$$\begin{aligned} \frac{\partial u_2^r}{\partial X} &= -\frac{PL_1^2}{2EI} - \frac{P(L-L_1)L_1}{EI} + \frac{2a(M_1+P_1 b)}{EI_t} - \frac{P_1(2a)^2}{2EI_t} - \frac{PL_3^2}{2EI} \\ &= -\frac{PL_1^2}{2EI} - \frac{P(L-L_1)L_1}{EI} + \frac{2M_1 a}{EI_t} - \frac{PL_3^2}{2EI} \end{aligned} \tag{17}$$

The traction vector components T_i for segment CD are given by

$$T_1 = \sigma_{11} n_1 + \sigma_{12} n_2 = \sigma_{11}, \; T_2 = \sigma_{21} n_1 + \sigma_{22} n_2 = \sigma_{21} \tag{18}$$

Use of Eqs. (15)-(18) in Eq. (14) yields

$$J^r_{CD}=\int_{CD}\left(W^r_{CD}-\left(T_1\frac{\partial u^r_1}{\partial X}+T_2\frac{\partial u^r_2}{\partial X}\right)\right)\mathrm{d}s=-\int_{CD}\tau^r_{xy4}\frac{\partial u^r_2}{\partial X}\mathrm{d}s=\frac{\partial u^r_2}{\partial X}P \tag{19}$$

By a static FE analysis [31,47] and experimental validation [31], one can find that the curvature of the static deflection of a cantilever beam at the center of a horizontal crack is the same as that of the corresponding beam without the crack:

$$\frac{\partial^2 Y_t}{\partial X^2}=\frac{\partial^2 Y_b}{\partial X^2}=\frac{\partial^2 Y_h}{\partial X^2} \tag{20}$$

where Y_t and Y_b are the displacements of the top and bottom segments of X_1X_2, respectively, and Y_h is the displacement of the corresponding beam without the crack. Hence

$$\frac{M_1}{EI_t}=\frac{M_2}{EI_b}=\frac{M_c}{EI} \tag{21}$$

Consequently, one has

$$M_1=\frac{I_tM_c}{I},\qquad M_2=\frac{I_bM_c}{I} \tag{22}$$

By moment balance of the right part of the beam at point B, one has

$$M_c-M_1-M_2+\frac{N_2(h-h_1)}{2}+N_1\left(h-\frac{h_1}{2}\right)=0 \tag{23}$$

where $M_c=-P(L-X_c)$ and $N_2=-N_1$. Hence

$$N_2=-N_1=-\frac{2M_c}{h}\left(1-\frac{I_t+I_b}{I}\right)=\frac{6h_1P(L-X_c)(h-h_1)}{h^3} \tag{24}$$

By force balance of the right part of the beam in the Y direction, one has

$$P_1+P_2=P \tag{25}$$

By deflection compatibility of the beam at the cross-section at X_2, i.e., the deflection along the centroidal axis of the top segment of X_1X_2 in the Y direction at X_2 relative to that at X_1 is the same as the deflection along the centroidal axis of the bottom segment of X_1X_2 in the Y direction at X_2 relative to that at X_1, one has

$$\frac{(M_1+P_1a)(2a)^2}{2EI_t}-\frac{P_1(2a)^3}{3EI_t}=\frac{(M_2+P_2a)(2a)^2}{2EI_b}-\frac{P_2(2a)^3}{3EI_b} \tag{26}$$

By Eqs. (24)-(26), one has

$$P_1=\frac{I_t}{I_t+I_b}P,\qquad P_2=\frac{I_b}{I_t+I_b}P \tag{27}$$

Substituting Eqs. (3), (12), (13), (17), (19), (21), (23), and (27) into Eq. (2) yields

$$\begin{aligned}J^r&=J^r_{AB}+J^r_{BC}+J^r_{CD}+J^r_{DE}+J^r_{EF}\\&=\frac{6(L-X_c)^2P^2}{Eh^3}+\frac{6(X_c-a)(2L-X_c+a)}{Eh^3}P^2-\frac{6L^2}{Eh^3}P^2\\&\quad+\frac{6a^2}{E\left[h_1^3+(h-h_1)^3\right]}P^2+\frac{12a(L-X_c)}{Eh^3}P^2\\&=\left(\frac{h^3}{h_1^3+(h-h_1)^3}-1\right)\frac{6a^2P^2}{Eh^3}\end{aligned} \tag{28}$$

The change in the strain energy caused by the horizontal crack is [19]

$$U^r_c=\int_0^a J^r(a)\mathrm{d}a \tag{29}$$

By Castigliano's theorem [22,23,61,62], the additional rotation θ caused by the horizontal crack at the cross-section at X_2 can be obtained:

$$\theta_r=\frac{\partial}{\partial P}\left[\int_0^a J^r(a)\mathrm{d}a\right]\frac{1}{\frac{\partial M_I}{\partial P}} \tag{30}$$

where $M_r=-P(L-(x_C+a))$ is the bending moment at the cross-section at X_2. By Eqs. (28) and (30), the equivalent rotational flexibility coefficient of the cross-section at X_2 is

$$c_2=\frac{\partial\theta_r}{\partial P}\frac{1}{\frac{\partial M_r}{\partial P}}=\frac{ba^3}{3EI(L-(X_c+a))^2}\left(\frac{h^3}{h_1^3+(h-h_1)^3}-1\right) \tag{31}$$

The rotational flexibility of the cross-section at X_2 can be modeled by a compliance c_2.

Proceeding in a similar manner, one can obtain the J-integral along the contour FEDCBA of the left part of the beam (see Appendix A for more details):

$$J^I=J^I_{AB}+J^I_{BC}+J^I_{CD}+J^I_{DE}+J^I_{EF}=\left(\frac{h^3}{h_1^3+(h-h_1)^3}-1\right)\frac{6a^2P^2}{Eh^3} \tag{32}$$

which is the same as that in Eq. (28). The additional rotation θ caused by the horizontal crack at the cross-section at X_1 is

$$\theta_l=\frac{\partial}{\partial P}\left[\int_0^b J^I(a)\mathrm{d}a\right]\frac{1}{\frac{\partial M_l}{\partial P}} \tag{33}$$

where $M_l=-P(L-(x_C-a))$ is the bending moment at the cross-section at X_1. The equivalent rotational flexibility of the cross-section at X_1 is

$$c_1=\frac{\partial\theta_l}{\partial P}\frac{1}{\frac{\partial M_l}{\partial P}}=\frac{ba^3}{3EI(L-(X_c-a))^2}\left(\frac{h^3}{h_1^3+(h-h_1)^3}-1\right) \tag{34}$$

The rotational flexibility of the cross-section at X_1 can be modeled by a compliance c_1. It can be seen from Eqs. (31) and (34) that $c_1=c_2=0$ when $a=0$ or $h_1=0$, as expected, and $c_1>c_2$. The nondimensional compliances are $c_1^*=EIc_1/Lt_1^2$ and $c_2^*=EIc_2/Lt_1^2$.

3. Free vibration analysis of a three-segment beam model

When the crack remains closed, the top and bottom segments of X_1X_2 have the same transverse displacements, but they can slide over each other in the axial direction except at their ends [16]. Hence the top and bottom segments of X_1X_2 can be considered as one beam segment whose cross-sectional area moment of inertia is the sum of those of the top and bottom segments. Under the assumption that the ratio of the length of each beam segment to its height is relatively large, the cantilever beam with a closed, embedded horizontal crack can be modeled as a three-segment beam with local flexibilities at X_1 and X_2, whose compliances are c_1 and c_2, respectively, as shown in Fig. 3, and each beam segment can be modeled as an Euler–Bernoulli beam. The transverse displacement of the kth ($k=1, 2, 3$) segment of the beam is denoted by $Y_k(X, T)$ with $X_{k-1}<X<X_k$.

According to Euler Bernoulli beam theory [12,16,25–28], the equations of motion of the three beam segments are given by

$$EI\frac{\partial^4Y_k(X,T)}{\partial X^4}+\rho A\frac{\partial^2Y_k(X,T)}{\partial T^2}=0,\ X_{k-1}<X<X_k,\ k=1,3 \tag{35}$$

$$E(I_t+I_b)\frac{\partial^4Y_2(X,T)}{\partial X^4}+\rho A\frac{\partial^2Y_2(X,T)}{\partial T^2}=0,\ X_1<X<X_2 \tag{36}$$

where I is the cross-sectional area moment of inertia of the first and third segments of the beam, ρ is their mass density, A is their cross-sectional area, and $A_t+A_b=A$ has been used in Eq. (36). Note that $I_t+I_b<I$; hence the middle beam segment has a reduced cross-sectional area moment of inertia. Consequently, $E(I_t+I_b)<EI$; hence the middle beam segment has a reduced bending moment. The boundary conditions of the beam are [26,27]

$$Y_1(0,T)=Y_1'(0,T)=0,\qquad Y_3''(0,T)=Y_3'''(L,T)=0 \tag{37}$$

The continuity conditions at the cross-sections at X_1 and X_2 are [16]

$$Y_1(X_1^-,T)=Y_2(X_1^+,T)$$
$$Y_2(X_2^-,T)=Y_3(X_2^+,T)$$

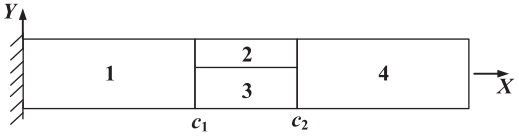

Fig. 3. Schematic of a three-segment beam model with compliances c_1 and c_2 at crack tips.

$$\begin{aligned} Y_1'(X_1^-,T) &= Y_2'(X_1^+,T)\\ Y_1'(X_2^+,T) &= Y_2'(X_2^-,T)\\ -EIY_1'''(X_1^-,T) &= -E(I_t+I_b)Y_2'''(X_1^+,T)\\ -EIY_3'''(X_2^-,T) &= -E(I_t+I_b)Y_2'''(X_2^+,T) \end{aligned} \tag{38}$$

The compatibility conditions of bending moments at X_1 and X_2 are

$$\begin{aligned} -EIY_2''(X_1^-,T) &= -(1+c_1^*)(EI_t+EI_b)Y_2''(X_1^+,T)\\ &\quad+\left(\frac{EA_tA_bh^2}{4L_2(A_t+A_b)}\right)(Y_1'(X_1^-,T)-Y_3'(X_2^+,T))\\ -EIY_3''(X_2^-,T) &= -(1+c_2^*)(EI_t+EI_b)Y_2''(X_2^+,T)\\ &\quad+\left(\frac{EA_tA_bh^2}{4L_2(A_t+A_b)}\right)(Y_1'(X_1^-,T)-Y_3'(X_2^+,T)) \end{aligned} \tag{39}$$

The following nondimensional quantities are introduced:

$$y=\frac{Y}{L},\quad x=\frac{X}{L},\quad x_k=\frac{X_k}{L},\quad l_1=\frac{L_1}{L},\quad l_2=\frac{L_2}{L},\quad l_3=\frac{L_3}{L} \tag{40}$$

Let $t=\sqrt{\frac{\rho AL^4}{EI}}$; Eqs. (35) and (36) become

$$EI\frac{\partial^4 y_k(x,t)}{\partial x^4}+\rho A\frac{\partial^2 y_k(x,t)}{\partial t^2}=0,\quad x_{k-1}<x<x_k,\quad k=1,3 \tag{41}$$

$$E(I_t+I_b)\frac{\partial^4 y_2(x,t)}{\partial x^4}+\rho A\frac{\partial^2 y_2(x,t)}{\partial t^2}=0,\quad x_1<x<x_2 \tag{42}$$

Let $y_k(x,t)=w_k(x)e^{i\omega t}$, where ω is the natural frequency, and $w_k(x)$ is the mode shape of the kth segment of the beam, Eqs. (41) and (42) become

$$w_k''''(x)-\lambda_k^4 w_k(x)=0,\quad x_{k-1}<x<x_k,\quad k=1,\ 2,\ 3 \tag{43}$$

where

$$\lambda_1^4=\frac{\rho A\omega^2L^4}{EI},\quad \lambda_2^4=\frac{\rho A\omega^2L^4}{E(I_t+I_b)},\quad \lambda_3^4=\frac{\rho A\omega^2L^4}{EI} \tag{44}$$

Let $\Lambda=\frac{EA_tA_bh^2}{4L_2(A_t+A_b)}$, $I_l=(1+c_1^*)(I_t+I_b)$, and $I_r=(1+c_2^*)(I_t+I_b)$; the continuity and compatibility conditions in Eqs. (38) and (39) become

$$\begin{aligned} w_1(x_1^-) &= w_2(x_1^+)\\ w_2(x_2^-) &= w_3(x_2^+)\\ w_1'(x_1^-) &= w_2'(x_1^+)\\ w_2'(x_2^-) &= w_3'(x_2^+)\\ -EIw_1'''(x_1^-) &= -E(I_t+I_b)w_2'''(x_1^+)\\ -EIw_3'''(x_2^-) &= -E(I_t+I_b)w_2'''(x_2^+)\\ -EIw_1''(x_1^-) &= -EI_lw_2''(x_1^+)+\Lambda(w_1'(x_1^-)-w_3'(x_2^+))\\ -EIw_3''(x_2^+) &= -EI_rw_2''(x_2^+)+\Lambda(w_1'(x_1^-)-w_3'(x_2^+)) \end{aligned} \tag{45}$$

The general solution of Eq. (43) for each segment of the beam is

$$\begin{aligned} w_k(x) &= A_k'\sin\lambda_k(x-x_{k-1})+B_k'\cos\lambda_k(x-x_{k-1})\\ &\quad+C_k'\sinh\lambda_k(x-x_{k-1})+D_k'\cosh\lambda_k(x-x_{k-1}),\quad x_{k-1}<x<x_k,\quad k=1,2,3 \end{aligned} \tag{46}$$

where A_k', B_k', C_k', and D_k' are unknown constants associated with the kth segment of the beam for each natural frequency. By Eq. (45), one can relate the unknown constants associated with the $(k+1)$th segment of the beam to those associated with the kth segment:

$$\begin{bmatrix} t_{11}^k & t_{12}^k & t_{13}^k & t_{14}^k\\ t_{21}^k & t_{22}^k & t_{23}^k & t_{24}^k\\ t_{31}^k & t_{32}^k & t_{33}^k & t_{34}^k\\ t_{41}^k & t_{42}^k & t_{43}^k & t_{44}^k \end{bmatrix}\begin{Bmatrix} A_k'\\ B_k'\\ C_k'\\ D_k' \end{Bmatrix}=\begin{bmatrix} t_{11}^{k+1} & t_{12}^{k+1} & t_{13}^{k+1} & t_{14}^{k+1}\\ t_{21}^{k+1} & t_{22}^{k+1} & t_{23}^{k+1} & t_{24}^{k+1}\\ t_{31}^{k+1} & t_{32}^{k+1} & t_{33}^{k+1} & t_{34}^{k+1}\\ t_{41}^{k+1} & t_{42}^{k+1} & t_{43}^{k+1} & t_{44}^{k+1} \end{bmatrix}\begin{Bmatrix} A_{k+1}'\\ B_{k+1}'\\ C_{k+1}'\\ D_{k+1}' \end{Bmatrix} \tag{47}$$

Let

$$\mathbf{T}_1=\begin{bmatrix} \sin\lambda_1 l_1 & \cos\lambda_1 l_1 & \sinh\lambda_1 l_1 & \cosh\lambda_1 l_1 \\ \lambda_1\Lambda\cos\lambda_1 l_1-EI\lambda_1^2\sin\lambda_1 l_1 & -\lambda_1\Lambda\sin\lambda_1 l_1-EI\lambda_1^2\cos\lambda_1 l_1 & \lambda_1\Lambda\cosh\lambda_1 l_1+EI\lambda_1^2\sinh\lambda_1 l_1 & EI\lambda_1^2\cosh\lambda_1 l_1+\lambda_1\Lambda\sinh\lambda_1 l_1 \\ -EI\lambda_1^3\cos\lambda l_1 & EI\lambda_1^3\sin\lambda l_1 & EI\lambda_1^3\cosh\lambda l_1 & EI\lambda_1^3\sinh\lambda l_1 \\ \lambda_1\cos\lambda_1 l_1 & -\lambda_1\sin\lambda_1 l_1 & \lambda_1\cosh\lambda_1 l_1 & \lambda_1\sinh\lambda_1 l_1 \end{bmatrix} \tag{48}$$

$$\mathbf{T}_2=\begin{bmatrix} 0 & 1 & 0 & 1 \\ \lambda_2\Lambda\cos\lambda_2 l_2 & -EI_l\lambda_2^2-\lambda_2\Lambda\sin\lambda_2 l_2 & \lambda_2\Lambda\cosh\lambda_2 l_2 & \lambda_2\Lambda\sinh\lambda_2 l_2+EI_l\lambda_2^2 \\ -\lambda_2^3E(I_t+I_b) & 0 & \lambda_2^3E(I_t+I_b) & 0 \\ \lambda_2 & 0 & \lambda_2 & 0 \end{bmatrix} \tag{49}$$

$$\mathbf{T}_3=\begin{bmatrix} \sin\lambda_2 l_2 & \cos\lambda_2 l_2 & \sinh\lambda_2 l_2 & \cosh\lambda_2 l_2 \\ -\lambda_2\Lambda-EI_r\lambda_2^2\sin\lambda_2 l_2 & -EI_r\lambda_2^2\cos\lambda_2 l_2 & -\lambda_2\Lambda+EI_r\lambda_2^2\sinh\lambda_2 l_2 & EI_r\lambda_2^2\cosh\lambda_2 l_2 \\ -E(I_t+I_b)\lambda_2^3\cos\lambda_2 l_2 & E(I_t+I_b)\lambda_2^3\sin\lambda_2 l_2 & E(I_t+I_b)\lambda_2^3\cosh\lambda_2 l_2 & E(I_t+I_b)\lambda_2^3\sinh\lambda_2 l_2 \\ \lambda_2\cos\lambda_2 l_2 & -\lambda_2\sin\lambda_2 l_2 & \lambda_2\cosh\lambda_2 l_2 & \lambda_2\sinh\lambda_2 l_2 \end{bmatrix} \tag{50}$$

$$\mathbf{T}_4=\begin{bmatrix} 0 & 1 & 0 & 1 \\ -\lambda_3\Lambda & -EI\lambda_3^2 & -\lambda_3\Lambda & EI\lambda_3^2 \\ -EI\lambda_3^3 & 0 & EI\lambda_3^3 & 0 \\ \lambda_3 & 0 & \lambda_3 & 0 \end{bmatrix} \tag{51}$$

Then

$$\begin{Bmatrix} A_2' \\ B_2' \\ C_2' \\ D_2' \end{Bmatrix}=\mathbf{T}_2^{-1}\mathbf{T}_1\begin{Bmatrix} A_1' \\ B_1' \\ C_1' \\ D_1' \end{Bmatrix} \tag{52}$$

$$\begin{Bmatrix} A_3' \\ B_3' \\ C_3' \\ D_3' \end{Bmatrix}=\mathbf{T}_4^{-1}\mathbf{T}_3\mathbf{T}_2^{-1}\mathbf{T}_1\begin{Bmatrix} A_1' \\ B_1' \\ C_1' \\ D_1' \end{Bmatrix} \tag{53}$$

Furthermore, the boundary conditions in Eq. (37) are reduced to

$$w(0)=0,\quad w'(0)=0 \tag{54}$$

$$w''(1)=0,\quad w'''(1)=0 \tag{55}$$

Applying the boundary conditions in Eq. (54) to Eq. (46) yields

$$A_1'+C_1'=0,\quad B_1'+D_1'=0 \tag{56}$$

Applying the boundary conditions in Eq. (55) to Eq. (46) yields

$$-\lambda_3^2A_3'\sin\lambda_3(l_3)-\lambda_3^2B_3'\cos\lambda_3(l_3)+\lambda_3^2C_3'\sinh\lambda_3(l_3)+\lambda_3^2D_3'\cosh\lambda_3(l_3)=0 \tag{57}$$

$$-\lambda_3^3A_3'\cos\lambda_3(l_3)+\lambda_3^3B_3'\sin\lambda_3(l_3)+\lambda_3^3C_3'\cosh\lambda_3(l_3)+\lambda_3^3D_3'\sinh\lambda_3(l_3)=0 \tag{58}$$

Eqs. (57) and (58) can be written in the matrix form

$$\mathbf{B}\begin{Bmatrix} A_3' \\ B_3' \\ C_3' \\ D_3' \end{Bmatrix}=\begin{Bmatrix} 0 \\ 0 \end{Bmatrix} \tag{59}$$

where

$$\mathbf{B}=\begin{bmatrix} -\sin\lambda_3(l_3) & -\cos\lambda_3(l_3) & \sinh\lambda_3(l_3) & \cosh\lambda_3(l_3) \\ -\cos\lambda_3(l_3) & \sin\lambda_3(l_3) & \cosh\lambda_3(l_3) & \sinh\lambda_3(l_3) \end{bmatrix} \tag{60}$$

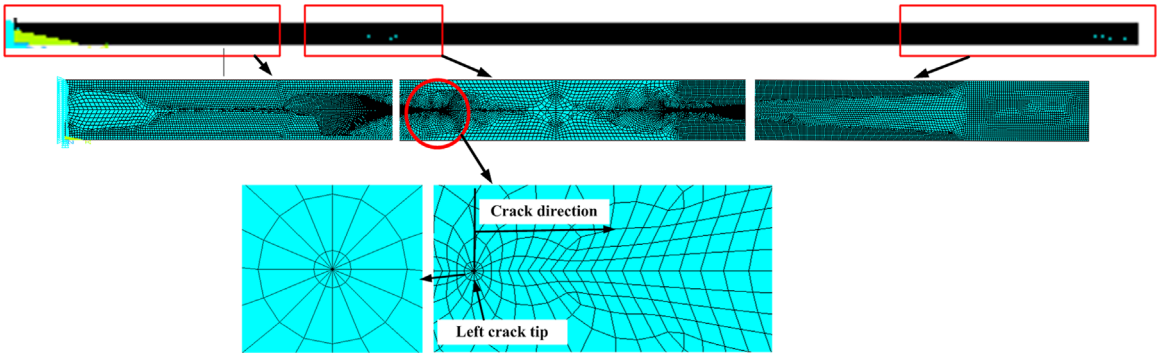

Fig. 4. FE model of a cracked cantilever beam.

Substituting Eq. (53) into (59) yields

$$\begin{Bmatrix} 0 \\ 0 \end{Bmatrix} = \mathbf{B} \begin{Bmatrix} A_3' \\ B_3' \\ C_3' \\ D_3' \end{Bmatrix} = \mathbf{B}\mathbf{T}_4^{-1}\mathbf{T}_3\mathbf{T}_2^{-1}\mathbf{T}_1 \begin{Bmatrix} A_1' \\ B_1' \\ C_1' \\ D_1' \end{Bmatrix} \tag{61}$$

Let

$$\mathbf{R} = \mathbf{B}\mathbf{T}_4^{-1}\mathbf{T}_3\mathbf{T}_2^{-1}\mathbf{T}_1 = \begin{bmatrix} R_{11} & R_{12} & R_{13} & R_{14} \\ R_{21} & R_{22} & R_{23} & R_{24} \end{bmatrix} \tag{62}$$

Use of Eqs. (56), (61), and (62) yields

$$\begin{bmatrix} R_{11}-R_{13} & R_{12}-R_{14} \\ R_{21}-R_{23} & R_{22}-R_{24} \end{bmatrix} \begin{Bmatrix} A_1' \\ B_1' \end{Bmatrix} = \begin{Bmatrix} 0 \\ 0 \end{Bmatrix} \tag{63}$$

Existence of a non-trivial solution of Eq. (63) requires

$$\det \begin{bmatrix} R_{11}-R_{13} & R_{12}-R_{14} \\ R_{21}-R_{23} & R_{22}-R_{24} \end{bmatrix} = 0 \tag{64}$$

which is the frequency equation of the three-segment beam model $f(\omega)=0$. The natural frequencies of the beam ω_n, where n is the mode number, can be obtained from the frequency equation using Newton–Raphson method. The initial guesses of ω_n are chosen to be close to the roots of the frequency equation, which can be obtained by plotting the function $f(\omega)$ and finding the approximate roots of $f(\omega)=0$. By Eqs. (48)-(53), (61), and (64), and assuming B_1' has an arbitrary known value, one can obtain all the other constants of A_k', B_k', C_k', and D_k' ($k=1, 2, 3$) in $w_k(x)$ in Eq. (46). The normalized mode shapes of the beam are defined by

$$\hat{w}_n(x) = \frac{w_n(x)}{\max(w_n(x))} \tag{65}$$

4. Numerical results

4.1. Verification of the J-integrals

To verify the analytical expressions of the J-integrals in Eqs. (28) and (32), nondimensional numerical results of the J-integrals surrounding the two crack tips are calculated using commercial FE software [57]. Two-dimensional (2D) singular elements PLANE183, which are six-node shell elements with two degrees of freedom at each node, are used around the crack tips of the cantilever beam. The other parts of the beam are modeled using 2D plane strain solid elements PLANE42. The FE model of a cracked cantilever beam is shown in Fig. 4. The parameters used are $P=1$, $E=1$, $h/L=0.05$, and $L_2/L=0.1$, with various ratios of X_c/L and h_1/h; the Poisson's ratio of the beam is assumed to be $\nu=0.3$. Table 1 shows the comparison of the nondimensional plane stress results of the J-integrals corresponding to the right and left crack tips from the FE method, which are obtained by dividing the calculated plane strain ones by $1-\nu^2$, and the nondimensional results of the J-integrals corresponding to the right and left crack tips defined by $\widehat{J} = \left(Eh^3/\left(P^2L^2\right)\right)J^r = \left(Eh^3/\left(P^2L^2\right)\right)J^l$, where J^r and J^l are determined by Eqs. (28) and (32), respectively. Since there are small differences between the FE results of the J-integrals

corresponding to the right and left crack tips, their mean values are compared with the analytical results. The numerical results show that the differences between the two methods are less than 3.8%, which demonstrates that Eqs. (28) and (32) are valid for Euler–Bernoulli beam segments. Since the top and bottom segments are assumed to have the same transverse displacements and they can slide over each other in the axial direction except at their ends, the stress intensity factors K_{II} from the FE and proposed methods are compared to verify the proposed J-integral approach, as shown in Table 2. The results show that the differences between the two methods are less than 2%, which further demonstrates that the proposed J-integral approach is valid for Euler–Bernoulli beam segments.

4.2. Effect of local flexibilities at crack tips on natural frequencies and mode shapes of a cracked cantilever beam

Consider a cracked cantilever beam with $L=600$ mm, $h=b=10$ mm, $E=2.06\times10^{11}$ N/m^2, and $\rho=7800$ kg/m^3. The first three natural frequencies of the beam without the crack are $\omega_{01}=23.060$ Hz, $\omega_{02}=144.516$ Hz, and $\omega_{03}=404.649$ Hz. The ratios of the first three natural frequencies of the three-segment beam and the corresponding one without local flexibilities at the crack tips to those of the beam without the crack are compared, as shown in Table 3. While the natural frequencies from the three-segment beam models with and without local flexibilities at the crack tips decrease with the length and depth of the crack, the differences between the natural frequencies from the three-segment beam models with and without local flexibilities at the crack tips range from 0.048% to 2.949%.

Fig. 5 shows the comparison of the first three normalized mode shapes of the cracked cantilever beam with $X_1/L=0.25$, $h_1/h=0.4$, and $L_2/L=0.1$ from the three-segment beam models with and without local flexibilities at the crack tips (a–c) and their single-level SWT decomposition detail coefficients [58,59] calculated using the MATLAB program SWT (d–f); the crack is located between points A and B, and the normalized mode shapes from the three-segment beam model without local flexibilities at the crack tips can be obtained from the results in Section 3 with $c_1=c_2=0$. The differences between the first three normalized mode shapes from the two models in Fig. 5(a–c) increase with the crack length, as well as those between the corresponding SWT decomposition detail coefficients of the three mode shapes in (d–f). The effects of the local flexibilities at the crack tips on the first three mode shapes and their SWT decomposition detail coefficients increase with the crack length. Hence, the local flexibilities at the crack tips should be considered in the cantilever beam model.

4.3. Effects of the crack length, location, and depth on the mode shapes of the cracked cantilever beam

The effects of the crack length, location, and depth on single-level SWT decomposition detail coefficients of the first three normalized mode shapes of the cracked cantilever beam are shown in Figs. 6–8, respectively. The crack lengths and locations can be clearly and directly identified from kinks in the single-level SWT decomposition detail coefficients of the first three normalized mode shapes of the beam, where the cracks are located between points a and b, points a and c, and points a and d in Fig. 6; between points a and d, points b and e, and c and f in Fig. 7; and between points a and b in Fig. 8. It can be seen that the amplitudes of the kinks slightly increase with the crack depth in Fig. 8.

5. Experimental validation and numerical verification

To validate the three-segment beam model, a cracked acrylonitrile butadiene styrene beam of length 111.4 mm, height 5.2 mm, and width 10.5 mm is made by a 3D printer, as shown in Fig. 9(a). The length, height, and width of a horizontal, rectangular crack are 16.6 mm, 0.3 mm, and 10.5 mm, respectively, as shown in Fig. 9(b). The distance between the left end of the crack and the fixed end of the beam is 53.1 mm, and that between the top surface of the crack and the top surface of beam is 2.6 mm.

An experimental setup is shown in Fig. 10. An operational modal analysis with non-contact excitation and measurement is performed on the cracked beam. An electric speaker is used to generate acoustic excitation to the beam. Two Doppler laser vibrometers are used to measure the response of the beam: Laser 1 and Laser 2 measure velocities of measurement points

Table 1
Comparison of the nondimensional results of the J-integrals corresponding to the right and left crack tips from the FE method and Eqs. (28) and (32), respectively.

X_c/L	h_1/h	FE method			Eqs. (28) and (32)	Difference (%)
		Right	Left	Mean value		
0.4	0.3	0.0257	0.0273	0.0265	0.0255	3.77
0.5	0.3	0.0258	0.0266	0.0262	0.0255	2.67
0.6	0.3	0.0265	0.0262	0.0264	0.0255	3.41
0.4	0.4	0.0386	0.0412	0.0399	0.0386	3.26
0.5	0.4	0.0390	0.0387	0.0389	0.0386	0.77
0.6	0.4	0.0392	0.0390	0.0391	0.0386	1.28

Table 2
Comparison of the stress intensity factors K_{II} at the right and left crack tips from the FE and proposed methods.

X_c/L	h_1/h	FE method			Proposed method	Difference (%)
		Right	Left	Mean value		
0.4	0.3	15.031	15.492	15.263	14.973	1.90
0.5	0.3	15.060	15.292	15.177	14.973	1.34
0.6	0.3	15.263	15.177	15.220	14.973	1.63
0.4	0.4	18.421	19.032	18.729	18.421	1.64
0.5	0.4	18.516	18.445	18.481	18.421	0.32
0.6	0.4	18.563	18.516	18.540	18.421	0.64

Table 3
Comparison between the first three natural frequencies from the three-segment beam models with and without local flexibilities at the crack tips.

$X_1/L \times h_1/h$	L_2/L	Three-segment beam models	Natural frequency ratios		
			ω_1/ω_{01}	ω_2/ω_{02}	ω_3/ω_{03}
0.25×0.4	0.1	With local flexibilities	0.861	0.958	0.881
		Without local flexibilities	0.857	0.959	0.879
		Difference (%)	0.431	0.068	0.224
0.25×0.4	0.15	With local flexibilities	0.835	0.914	0.868
		Without local flexibilities	0.820	0.915	0.863
		Difference (%)	1.837	0.048	0.551
0.2×0.2	0.2	With local flexibilities	0.902	0.957	0.920
		Without local flexibilities	0.890	0.961	0.915
		Difference (%)	1.435	0.385	0.577
0.2×0.3	0.2	With local flexibilities	0.844	0.930	0.885
		Without local flexibilities	0.820	0.936	0.878
		Difference (%)	2.949	0.582	0.814

and the velocity of a reference point on the beam, respectively. There are totally 129 measurement points on the beam, which are evenly distributed along the length of beam. The third natural frequency and mode shape of the cracked beam are measured using Operational PloyMax of LMS Test. Lab Rev. 9b.

The third natural frequencies form the experiment, the FE model, and the three-segment beam model are 1608 Hz, 1604.3 Hz, and 1600.7 Hz, respectively. The difference between the third natural frequency from the FE model and the experiment is -0.25%, and that between the three-segment beam and the experiment is -0.45%. The fourth natural frequency form the experiment, the FE model, and the three-segment beam model are 3124.2 Hz, 3179 Hz, and 2966.8 Hz, respectively. The difference between the natural frequency from the FE model and the experiment is 1.72%, and that between the three-segment beam and the experiment is -5.03%. Fig. 11 shows the third and fourth normalized mode shapes from the experiment, the FE model, and the three-segment beam model and their SWT decomposition detail coefficients. The third and fourth normalized mode shapes and their SWT decomposition detail coefficients from the experiment agree very well with those from the FE model, and they are similar in shape to those from the three-segment beam model. The spatial regions with abrupt changes of the SWT decomposition detail coefficients of the third and fourth normalized mode shape from the experiment, the FE model, and the three-segment beam model correspond to the crack region, as shown in Fig. 11(c and d), which can be used to identify the crack length and location. The results from the experiment and the FE model validate and verify to some extent the three-segment beam model, respectively. Note that the results from the FE model are overall closer to those from the experiment than the three-segment beam model. One reason is that there is a non-zero height of the crack in the experiment and the FE model, which is not considered in the three-segment beam model. Note also that the proposed analytical method is useful even though the FE method is available. For example, such an analytical model can be easily implemented and run on a broad range of computational platforms, requiring minimal computational resources such as dedicated software, while also executed at minimal computational costs compared with the computational resources and costs required to run a fully tested FE model that can yield reliable convergent solutions.

6. Conclusion

A new three-segment beam model with local flexibilities at crack tips is developed to investigate the vibration of a cantilever beam with a closed, fully embedded horizontal crack. The effect of the crack is modeled by local flexibilities at the crack tips and a reduced bending moment of the middle segment of the beam containing the crack. The compliances at the

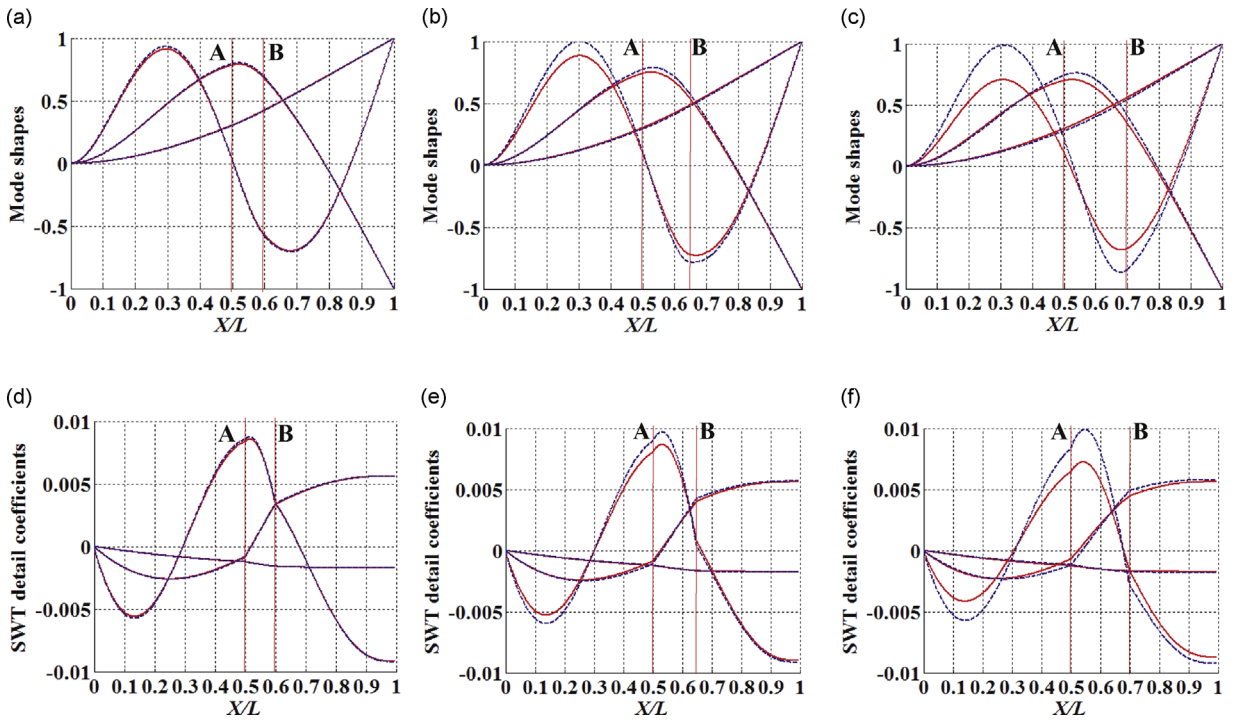

Fig. 5. Comparison of the first three normalized mode shapes from the three-segment beam models with (——) and without (– – –) local flexibilities at the crack tips and their SWT decomposition detail coefficients: (a) $X_1/L=0.5$, $L_2/L=0.1$, and $h_1/h=0.4$; (b) $X_1/L=0.5$, $L_2/L=0.15$, and $h_1/h=0.4$; (c) $X_1/L=0.5$, $L_2/L=0.2$, and $h_1/h=0.4$; (d) $X_1/L=0.5$, $L_2/L=0.1$, and $h_1/h=0.4$; (e) $X_1/L=0.5$, $L_2/L=0.15$, and $h_1/h=0.4$; and (f) $X_1/L=0.5$, $L_2/L=0.2$, and $h_1/h=0.4$ (To better distinguish different line types in this figure legend, the reader is referred to the web version of this article.).

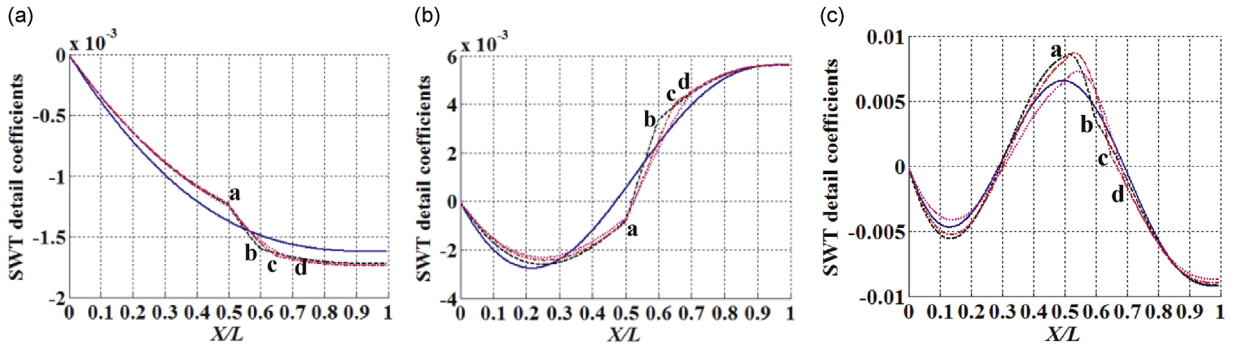

Fig. 6. Effect of the crack length on SWT decomposition detail coefficients of the first three normalized mode shapes of the beam with and without the crack: ——, the beam without the crack; – – –, $X_1/L=0.5$, $L_2/L=0.1$, and $h_1/h=0.4$; –·–, $X_1/L=0.5$, $L_2/L=0.15$, and $h_1/h=0.4$; · · ·, $X_1/L=0.5$, $L_2/L=0.2$, and $h_1/h=0.4$. (a) The first mode, (b) the second mode, and (c) the third mode. (To better distinguish different line types in this figure legend, the reader is referred to the web version of this article.)

crack tips are analytically determined using a *J*-integral approach. The natural frequencies and mode shapes of the three-segment beam with local flexibilities at the crack tips are derived using compatibility conditions at the crack tips and the transfer matrix method. The following conclusions can be obtained from this study:

1) The values of the *J*-integrals along the contours of the left and right parts of the beam are the same for Euler–Bernoulli beam segments. The equivalent rotational flexibility of the cross-section of the beam at the left crack tip is larger than that at the right tip. The differences between the *J*-integral results from the analytical and FE methods are less than 3.8%. The differences between the stress intensity factors K_{II} from the analytical and FE methods are less than 2%.
2) The differences between the natural frequencies from the three-segment beam models with and without local flexibilities at the crack tips range from 0.048% to 2.949%.

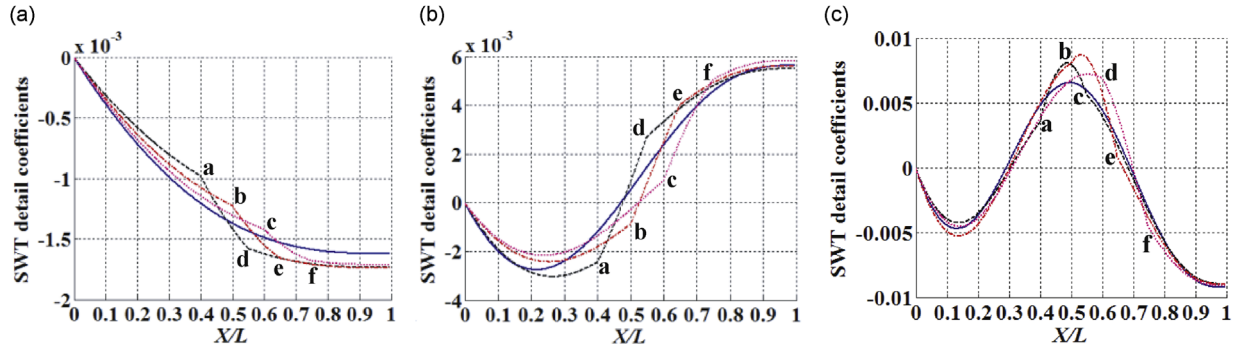

Fig. 7. Effect of the crack location on SWT decomposition detail coefficients of the first three normalized mode shapes of the beam with and without the crack: ——, the beam without the crack; – – –, $X_1/L=0.4$, $L_2/L=0.15$, and $h_1/h=0.4$; –·–, $X_1/L=0.5$, $L_2/L=0.15$, and $h_1/h=0.4$; · · ·, $X_1/L=0.6$, $L_2/L=0.15$, and $h_1/h=0.4$. (a) The first mode, (b) the second mode, and (c) the third mode. (To better distinguish different line types in this figure legend, the reader is referred to the web version of this article.)

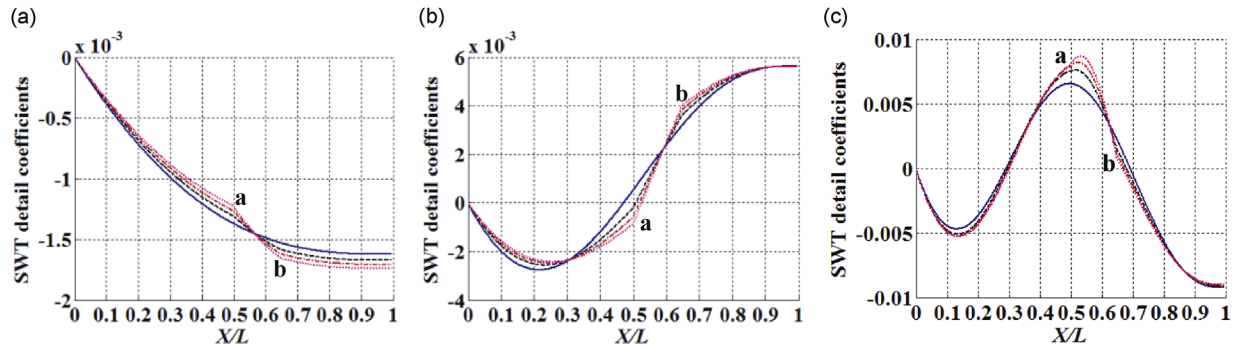

Fig. 8. Effect of the crack depth on SWT decomposition detail coefficients of the first three normalized mode shapes of the beam with and without the crack: ——, the beam without the crack; – – –, $X_1/L=0.5$, $L_2/L=0.15$, and $h_1/h=0.2$; –·–, $X_1/L=0.5$, $L_2/L=0.15$, and $h_1/h=0.3$; · · ·, $X_1/L=0.5$, $L_2/L=0.15$, and $h_1/h=0.4$. (a) The first mode, (b) the second mode, and (c) the third mode. (To better distinguish different line types in this figure legend, the reader is referred to the web version of this article.)

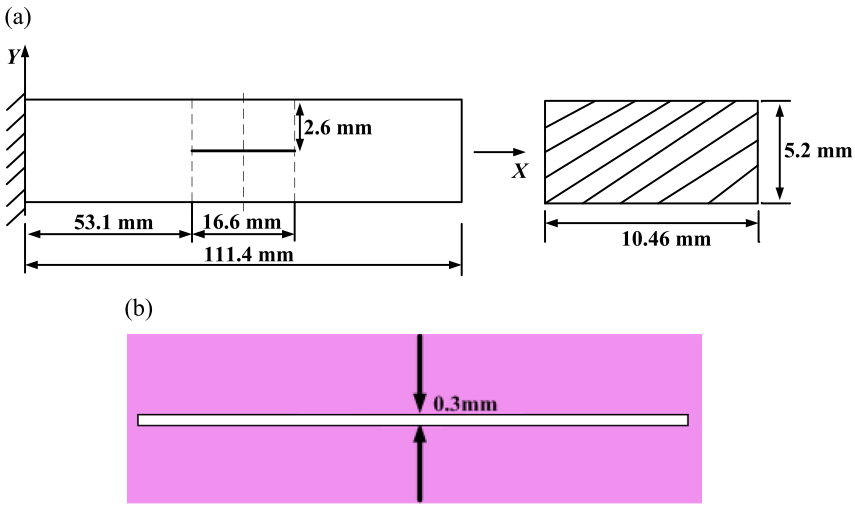

Fig. 9. (a) Dimensions of a cantilever beam with an embedded crack and (b) an enlarged view of the crack region.

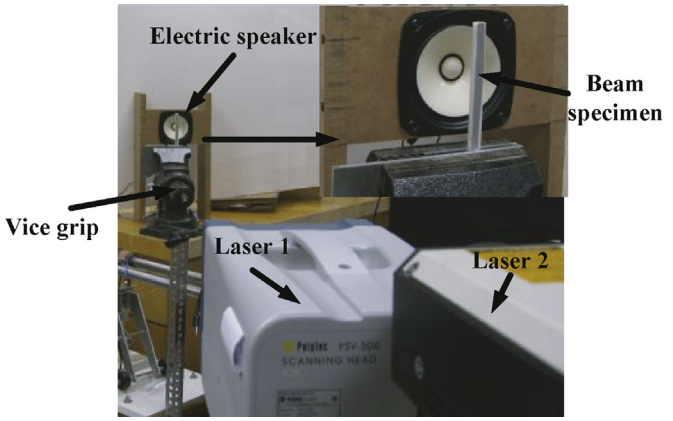

Fig. 10. An experimental setup for the cracked beam using operational modal analysis.

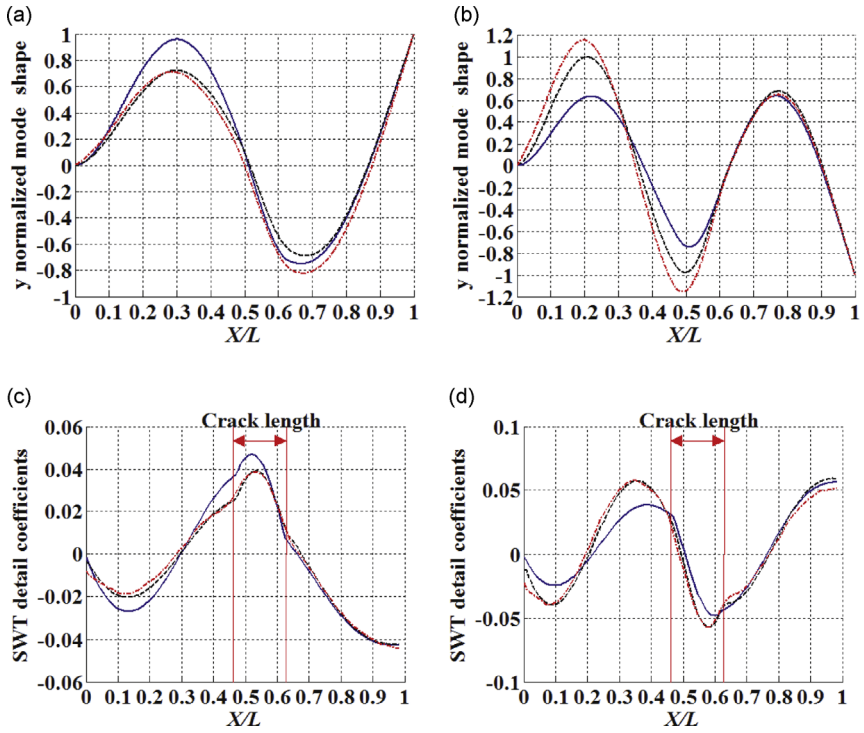

Fig. 11. The third normalized mode shapes from the experiment (-·-·-), the FE model (- - -), and the three-segment beam model (——) and their SWT decomposition detail coefficients: (a) the third mode shape; (b) the fourth mode shape; (c) SWT decomposition detail coefficients of the third mode shape; and (d) SWT decomposition detail coefficients of the fourth mode shape. (To better distinguish different line types in this figure legend, the reader is referred to the web version of this article.)

3) The differences between the first three normalized mode shapes from the three-segment beam models with and without local flexibilities at the crack tips increase with the crack length, as well as those between the corresponding SWT decomposition detail coefficients of the three mode shapes. The local flexibilities at the crack tips should be considered in the cantilever beam model.
4) The regions of abrupt changes of single-level SWT decomposition detail coefficients of normalized mode shapes of the cracked cantilever beam correspond to the crack region, which can be used to identify the length and location of a closed, fully embedded horizontal crack.

Acknowledgement

The authors are grateful for the financial support provided by the National Natural Science Foundation of China under Grant numbers 51475053 and 11442006, the National Science Foundation under Grant numbers CMMI-1000830, CMMI-

1229532, and CMMI-1335024, the University of Maryland Baltimore County Directed Research Initiative Fund Program, and the Fundamental Research Funds for the Central Universities.

Appendix A. Determination of the *J*-integral along the contour FEDCBA of the left part of the beam in Fig. 2(a)

The *J*-integral along the contour FEDCBA of the left part of the beam in Fig. 2(a) is the sum of line integrals along segments FE, ED, DC, CB, and BA of the contour:

$$J^l = J^l_{BA} + J^l_{CB} + J^l_{DC} + J^l_{ED} + J^l_{FE} \tag{A1}$$

where the superscript l denotes the left part. For segments CB and ED, $dY=0$ and $T_i=0$; hence

$$J^l_{CB} = 0, \quad J^l_{ED} = 0 \tag{A2}$$

For segment BA, one has

$$J^l_{BA} = \int_{BA} \left(W^l_{AB} dy - T_i \frac{\partial u_i}{\partial X} ds \right) = \int_{BA} \left(-W^l_{AB} ds - \left(T_1 \frac{\partial u^l_1}{\partial X} + T_2 \frac{\partial u^l_2}{\partial X} \right) ds \right) \tag{A3}$$

where

$$W^l_{BA} = \frac{1}{2}\sigma^l_{xx2}\varepsilon^l_{xx2} + \frac{1}{2}\tau^l_{xy2}\gamma^l_{xy2} \tag{A4}$$

in which σ^l_{xx2} and τ^l_{xy2} are the normal and shear stresses on segment BA, respectively, ε^l_{xx2} and γ^l_{xy2} are the normal and shear strains of segment BA, respectively, and the subscript 2 denotes the stress and strain components associated with segment BA. They are given by

$$\begin{aligned} \sigma^l_{xx2} &= \frac{N_2}{A_b} - \frac{M_2}{I_b} Y, \varepsilon^l_{xx2} = \frac{\partial u_1}{\partial X} = \frac{N_2}{EA_b} - \frac{M_2}{EI_b} Y \\ \tau^l_{xy2} &= \frac{P_2 S(Y)}{I_b t}, \gamma^l_{xy2} = \frac{\tau^l_{xy2}}{G} = \frac{\partial u^l_1}{\partial Y} + \frac{\partial u^l_2}{\partial X} = \frac{P_2 S(Y)}{G I_b t} \end{aligned} \tag{A5}$$

where u^l_1 and u^l_2 are the displacements of the beam segment of X_1X_2 in the X and Y directions, respectively. The relationship between the displacements in the X and Y directions is

$$u^l_1 = u^{0l}_1 - \frac{\partial u^{0l}_2}{\partial X} Y \tag{A6}$$

where the superscript 0 denotes deflections along the centroidal axis of the bottom segment of X_1X_2. Differentiating Eq. (A6) with respect to Y yields

$$\frac{\partial u^l_1}{\partial Y} = -\frac{\partial^2 u^{0l}_2}{\partial X \partial Y} Y - \frac{\partial u^{0l}_2}{\partial X} = -\frac{\partial u^{0l}_2}{\partial X} = -\frac{\partial u^l_2}{\partial X} \tag{A7}$$

where $\frac{\partial^2 u^{0l}_2}{\partial X \partial Y} = 0$. For the cracked cantilever beam, the rotational angle of the cross-section BA is assumed to be the sum of the rotational angle of the cross-section at X_1 relative to that at X_0 and the rotational angle of the cross-section at X_c relative to that at X_1:

$$\frac{\partial u^l_2}{\partial X} = -\frac{PL_1^2}{2EI} - \frac{P(L-L_1)L_1}{EI} - \frac{P_2 a^2}{2EI_b} + \frac{M_2 a}{EI_b} \tag{A8}$$

Then

$$\gamma^l_{xy2} = \frac{\partial u^l_2}{\partial X} = -\frac{PL_1^2}{2EI} - \frac{P(L-L_1)L_1}{EI} - \frac{P_2 a^2}{2EI_b} + \frac{M_2 a}{EI_b} \tag{A9}$$

The traction vector components for segment BA are given by

$$T_1 = \sigma_{11} n_1 + \sigma_{12} n_2 = -\sigma_{11}, \; T_2 = \sigma_{21} n_1 + \sigma_{22} n_2 = -\sigma_{21} \tag{A10}$$

Use of Eqs. (A4)–(A9) in Eq. (A3) yields

$$\begin{aligned} J^l_{BA} &= \int_{AB} \frac{1}{2}\sigma^l_{xx1}\epsilon^l_{xx1} \, dY + \int_{AB} \tau^l_{xy1} \frac{\partial u^l_1}{\partial X} dY \\ &= \frac{N_2^2}{2EA_b} + \frac{M_2^2}{2EI_b} + \frac{PP_2L_1^2}{2EI} + \frac{PP_2(L-L_1)L_1}{EI} + \frac{P_2^2 a^2}{2EI_b} + \frac{P_2 M_2 a}{EI_b} \end{aligned} \tag{A11}$$

Similarly, the line integral along segment FE is

$$J^l_{FE} = \int_{FE} \frac{1}{2}\sigma^l_{xx2}\epsilon^l_{xx2} dy + \int_{FE} \tau^l_{xy2} \frac{\partial u^l_2}{\partial X} dY$$

$$=\frac{N_1^2}{2EA_t}+\frac{M_1^2}{2EI_t}+\frac{PP_1L_1^2}{2EI}+\frac{PP_1(L-L_1)L_1}{EI}+\frac{P_1^2a^2}{2EI_t}+\frac{P_1M_1a}{EI_t} \tag{A12}$$

For segment DC

$$J_{DC}^l=\int_{DC}W_{DC}^l\mathrm{d}Y-T_i\frac{\partial u_i}{\partial X}\mathrm{d}s=\int_{DC}\left(W_{DC}^l-\left(T_1\frac{\partial u_1^l}{\partial X}+T_2\frac{\partial u_2^l}{\partial X}\right)\right)\mathrm{d}s \tag{A13}$$

where

$$W_{DC}^l=\frac{1}{2}\sigma_{xx4}^l\varepsilon_{xx4}^l+\frac{1}{2}\tau_{xy4}^l\gamma_{xy4}^l \tag{A14}$$

in which the subscript 4 denotes the stress and strain components associated with segment DC. The normal stress, normal strain, shear stress, and shear strain for segment DC are

$$\sigma_{xx4}^l(Y)=\frac{MY}{I},\quad \epsilon_{xx4}^l(Y)=\frac{\sigma_{xx4}^l}{E}=\frac{\partial u_1^l}{\partial X}=\frac{MY}{EI}$$
$$\tau_{xx4}^l=\frac{PS(Y)}{It_1},\quad \gamma_{xx4}^l=\frac{\tau_{xx4}^l}{G}=\frac{\partial u_1^l}{\partial Y}+\frac{\partial u_2^l}{\partial X}=\frac{PS(Y)}{GIt_1}=0 \tag{A15}$$

where $M=-PL$ is the bending moment at the cross-section at X_0. The traction vector components T_i for segment DC are

$$T_1=\sigma_{11}n_1+\sigma_{12}n_2=\sigma_{11},\ T_2=\sigma_{21}n_1+\sigma_{22}n_2=\sigma_{21} \tag{A16}$$

Use of Eqs. (A15) and (A16) in Eq. (13) yields

$$J_{DC}^l=\int_{DC}\left(W_{DC}^l-\left(T_1\frac{\partial u_1^l}{\partial X}+T_2\frac{\partial u_2^l}{\partial X}\right)\right)\mathrm{d}s$$
$$=\int_{DC}\left(\frac{1}{2}\sigma_{xx4}^l\epsilon_{xx4}^l+\frac{1}{2}\tau_{xx4}^l\gamma_{xx4}^l-\left(\sigma_{11}\frac{\partial u_1^l}{\partial X}+\sigma_{21}\frac{\partial u_2^l}{\partial X}\right)\right)\mathrm{d}s$$
$$=-\int_{DC}\frac{1}{2}\sigma_{xx4}^l\epsilon_{xx4}^l\,\mathrm{d}s=-\frac{6L^2}{Et_1h^3}P^2 \tag{A17}$$

Substituting Eqs. (A2), (A3), (A11), (A12), and (A17) into Eq. (A1) yields

$$J^l=J_{BA}^l+J_{CB}^l+J_{DC}^l+J_{ED}^l+J_{FE}^l=\left(\frac{h^3}{h_1^3+(h-h_1)^3}-1\right)\frac{6a^2P^2}{Eh^3} \tag{A18}$$

References

[1] W. Fan, P.Z. Qiao, Vibration-based damage identification methods: a review and comparative study, *Structural Health Monitoring* 10 (1) (2011) 83–111.
[2] Z.A. Jassim, N.N. Ali, F. Mustapha, N.A.A. Jalil, A review on the vibration analysis for a damage occurrence of a cantilever beam, *Engineering Failure Analysis* 31 (2013) 442–461.
[3] W.M. Ostachowicz, M. Krawczuk, Analysis of the effect of cracks on the natural frequencies of a cantilever beam, *Journal of Sound and Vibration* 150 (2) (1991) 191–201.
[4] K.H. Wang, D.J. Inman, C.R. Farrar, Modeling and analysis of a cracked composite cantilever beam vibrating in coupled bending and torsion, *Journal of Sound and Vibration* 284 (2005) 23–49.
[5] G. Hearn, Modal analysis for damage detection in structures, *Journal of Structural Engineering* 117 (10) (1991) 3042–3063.
[6] W.X. Ren, G.D. Roeck, Structural damage identification using modal data I: simulation verification, *Journal of Structural Engineering* 128 (1) (2002) 87–95.
[7] W.X. Ren, G.D. Roeck, Structural damage identification using modal data II: test verification, *Journal of Structural Engineering* 128 (1) (2002) 96–104.
[8] G.M. Owolabi, A.S.J. Swamidas, R. Seshadri, Crack detection in beams using changes in frequencies and amplitudes of frequency response functions, *Journal of Sound and Vibration* 265 (2003) 1–22.
[9] H. Nahvi, M. Jabbari, Crack detection in beams using experimental modal data and finite element model, *International Journal of Mechanical Sciences* 47 (2005) 1477–1497.
[10] N.T. Khiem, T.V. Lien, Multi-crack detection for beam by the natural frequencies, *Journal of Sound and Vibration* 273 (1) (2004) 175–184.
[11] A. Ouahabi, M. Thomas, A.A. Lakis, Detection of damages in beams and composite plates by harmonic excitation and time–frequency analysis, Proceedings of the 3rd European Workshop on Structural Health Monitoring, Granada, Spain, 2006.
[12] M.F. Yuen, A numerical study of the eigen parameters of a damaged cantilever, *Journal of Sound and Vibration* 103 (1985) 301–310.
[13] P.F. Rizos, N. Aspragathos, Identification of crack location and magnitude in a cantilever beam from the vibrating mode, *Journal of Sound and Vibration* 138 (3) (1990) 381–388.
[14] Y. Narkis, Identification of crack location in vibrating simply supported beams, *Journal of Sound and Vibration* 172 (4) (1994) 549–558.
[15] B.P. Nandwana, S.K. Maiti, Detection of the location and size of a crack in stepped cantilever beams based on measurements of natural frequencies, *Journal of Sound and Vibration* 203 (3) (1997) 435–446.
[16] S.I. Ishak, G.R. Liu, H.M. Shang, S.P. Lim, Non-destructive evaluation of forizontal crack detection in beams using transverse impact, *Journal of Sound and Vibration* 252 (2) (2002) 343–360.
[17] B. Li, X.F. Chen, J.X. Ma, Z.J. He, Detection of crack location and size in structures using wavelet finite element methods, *Journal of Sound and Vibration* 285 (4) (2005) 767–782.
[18] H.P. Lin, S.C. Chang, Forced response of cracked cantilever beams subjected to a concentrated moving load, *International Journal of Mechanical Sciences* 48 (2006) 1456–1463.
[19] A.S.Y. Alsabbagh, O.M. Abuzeid, M.H. Dado, Simplified stress correction factor to study the dynamic behavior of a cracked beam, *Applied Mathematical Modelling* 33 (1) (2009) 127–139.

[20] L. Rubio, An efficient method for crack identification in simply supported Euler–Bernoulli beams, *ASME Journal of Vibration and Acoustics* 131 (2009). 051001.
[21] M. Behzad, A. Meghdari, A. Ebrahimi, A new approach for vibration analysis of cracked beam, *International Journal of Engineering* 18 (4) (2005) 319–330.
[22] M. Behzad, A. Ebrahimi, A. Meghdari, A continuous vibration theory for beams with a vertical edge crack, *Transaction B Mechanical Engineering* 17 (3) (2010) 194–204.
[23] C.S. Wang, L.T. Lee, Modified and simplified sectional flexibility of a cracked beam, *Journal of Applied Mathematics* 2012 (2012) 1–16.
[24] X.B. Lu, J.K. Liu, Z.R. Lu, A two-step approach for crack identification in beam, *Journal of Sound and Vibration* 332 (2013) 282–293.
[25] T.G. Chondros, A.D. Dimarogonas, J. Yao, A continuous cracked beam vibration theory, *Journal of Sound and Vibration* 215 (1998) 17–34.
[26] E.I. Shifrin, R. Ruotolo, Natural frequencies of a beam with an arbitrary number of cracks, *Journal of Sound and Vibration* 222 (3) (1999) 409–423.
[27] H.P. Lin, S.C. Chang, J.D. Wu, Beam vibrations with arbitrary number of cracks, *Journal of Sound and Vibration* 258 (5) (2002) 987–999.
[28] J.T. Kim, N. Stubbs, Crack detection in beam-type structures using frequency data, *Journal of Sound and Vibration* 259 (1) (2003) 145–160.
[29] C.C. Chang, L.W. Chen, Detection of the location and size of cracks in the multiple cracked beam by spatial wavelet based approach, *Mechanical Systems and Signal Processing* 19 (1) (2005) 139–155.
[30] D.P. Patil, S.K. Maiti, Experimental verification of a method of detection of multiple cracks in beams based on frequency measurements, *Journal of Sound and Vibration* 281 (1) (2005) 439–451.
[31] P.M. Mujumdar, Suryanaryan, Flexural vibrations of beams with delaminations, *Journal of Sound and Vibration* 125 (3) (1988) 441–461.
[32] M.H.H. Shen, J.E. Grady, Free vibration of delaminated beams, *Aiaa Journal* 30 (5) (1992) 1361–1370.
[33] J. Lee, R.T. Haftka, O.H. Griffin, Detecting delaminations in a composite beam using anti-optimization, *Structural Optimization* 8 (2–3) (1994) 93–100.
[34] Q. Wang, X.M. Deng, Damage detection with spatial wavelets, *International Journal of Solids and Structures* 36 (1999) 3443–3468.
[35] H. Luo, S. Hanagud, Dynamics of delaminated beams, *International Journal of Solids and Structures* 37 (2000) 1501–1519.
[36] Y. Zou, L. Tong, G.P. Steven, Vibration-based model-dependent damage (delamination) identification and health monitoring for composite structures—a review, *Journal of Sound and Vibration* 230 (2) (2000) 357–378.
[37] J.H. Lee, Free vibration analysis of delaminated composite beams, *Computers and Structures* 74 (2000) 121–129.
[38] J. Wang, P. Qiao, Novel beam analysis of end notched flexure specimen for mode-II fracture, *Engineering Fracture Mechanics* 71 (2004) 219–231.
[39] Q. Wang, F. Moslehy, D.W. Nicholson, Stability analysis of a delaminated beam subjected to follower compression, *Aiaa Journal* 43 (9) (2005) 2052–2059.
[40] C.N. Della, D.W. Shu, Free vibration analysis of delaminated biomaterial beams, *Composite Structures* 80 (2007) 212–220.
[41] S.J. Wildy, A.G. Kotousov, B.S. Cazzolato, J.D. Codrington, New damage detection technique based on governing differential equations of continuum mechanics, Part I: out-of-plane loading, Proceedings of the 6th Australasian Congress on Applied Mechanics (ACAM 6), Perth, Australia, 2010.
[42] N. Wu, Q. Wang, Repair of vibrating delaminated beam structures using piezoelectric patches, *Smart Materials and Structures* 19 (2010) 035027.
[43] Q. Wang, N. Wu, Detecting the delaminations location of a beam with a wavelet transform: an experimental study, *Smart Materials and Structures* 20 (2011) 012002.
[44] N.H. Erdelyi, S.M. Hashemi, A dynamic stiffness element for free vibration analysis of delaminated layered beams, *Modelling and Simulation in Engineering* 2012 (2012) 492415.
[45] P.Z. Qiao, F.L. Chen, On the improved dynamic analysis of delaminated beams, *Journal of Sound and Vibration* 331 (2012) 1143–1163.
[46] X.D. Qian, M.S. Cao, Z.Q. Su, A hybrid particle swarm optimization (PSO)-simplex algorithm for damage identification of delaminated beams, *Mathematical Problems in Engineering* 2012 (2012) 1–11.
[47] X. Fang, *The Mechanics of an Elastically Deforming Cantilever Beam With an Embedded Sharp Crack and Subjected to an End Transverse Loading*, University of Maryland, Baltimore County, USA, 2013.
[48] J.R. Rice, A path independent integral and the approximate analysis of strain concentration by notches and cracks, *Journal of Applied Mechanics* 35 (1968) 379–386.
[49] L. Meirovitch, *Principles and Techniques of Vibrations*, Prentice Hall, New Jersey, 1997.
[50] S. Orhan, Analysis of free and forced vibration of a cracked cantilever beam, *NDTE International* 40 (2007) 443–450.
[51] S.C. Zhong, S.O. Yadiji, K. Ding, Response-only method for damage detection of beam-like structures using high accuracy frequencies with auxiliary mass spatial probing, *Journal of Sound and Vibration* 311 (2008) 1075–1099.
[52] J. Lee, Identification of multiple cracks in a beam using vibration amplitude, *Journal Sound and Vibration* 326 (1–2) (2009) 205–212.
[53] A.A. Masoud, S.A. Said, A new algorithm for crack location in a rotating Timoshenko beam, *Journal of Vibration and Control* 15 (10) (2009) 1541–1561.
[54] D.G. Kim, S.B. Lee, Structural damage identification of a cantilever beam using excitation force level control, *Mechanical Systems and Signal Processing* 24 (6) (2010) 1814–1830.
[55] M. Cao, L. Ye, L. Zhou, Sensitivity of fundamental mode shape and static deflection for damage identification in cantilever beams, *Mechanical Systems and Signal Processing* 25 (2) (2011) 630–643.
[56] N. Wu, Q. Wang, Experimental studies on damage detection of beam structures with wavelet transform, *International Journal of Engineering Science* 49 (3) (2011) 253–261.
[57] ANSYS Theory Reference, ANSYS Release 11.0: ANSYS, Inc., 2007.
[58] S. Zhong, S.O. Oyadiji, Crack detection in simply-supported beams without baseline model parameter by stationary wavelet transform, *Mechanical Systems and Signal Processing* 21 (4) (2007) 1853–1884.
[59] S.C. Zhong, J.Q. Guo, L.G. Yao, Y.Z. Zhuang, H.D. Lu, Wavelet-based damage localization in plate-like structures, Proceedings of the ASME 2012 International Mechanical Engineering Congress & Exposition, Texas, USA, 2012.
[60] I. Sharf, Nonlinear strain measures, shape functions and beam elements for dynamics of flexible beams, *Multibody System Dynamics* 3 (1999) 189–205.
[61] K. Hellan, *Introduction to Fracture Mechanics*, McGraw-Hill Inc, US, 1985.
[62] A.D. Dimarogonas, Vibration of cracked structures: a state of the art review, *Engineering Fracture Mechanics* 55 (5) (1996) 831–857.